Search for a correlation length in a simulation of the glass transition

Richard M. Ernst and Sidney R. Nagel
The James Franck Institute and The Department of Physics, The University of Chicago, Chicago, Illinois 60637

Gary S. Grest
Corporate Research Science Laboratory, Exxon Research and Engineering Company, Annandale, New Jersey 08801
(Received 26 November 1990)

We have looked for evidence of a correlation length in a molecular-dynamics simulation of the glass transition. We have studied the correlation functions of both the translational order of particle positions and the orientational order of nearest-neighbor bond angles, and have seen no indication of a diverging length scale. We also present data from the simulation, which extend recent laboratory measurements of the frequency-dependent specific heat and thermal conductivity.

I. INTRODUCTION

The glass transition, that is the freezing of a supercooled liquid into an amorphous solid, has thus far frustrated all attempts to characterize it as a thermodynamic phase transition. Many, perhaps all, liquids, when cooled sufficiently rapidly to below their equilibrium freezing temperatures, bypass crystallization and undergo such a transition into a glass. As a liquid is cooled towards the glass transition, its characteristic time scale grows rapidly, as measured by any of a number of experimental probes (such as viscosity or dielectric susceptibility). Eventually, it exceeds the laboratory time scale of the measurement itself; therein lies the difficulty in distinguishing a thermodynamic glass transition from kinetic freezing. One must distinguish between a divergence of the time scale at a nonzero temperature on the one hand from a time scale which merely continues to increase and which diverges at zero temperature on the other. The problem is that we cannot practically remain in equilibrium close to the apparent transition temperature. A major step toward resolving the dilemma would be the determination of an order parameter underlying the transition. The discovery of a diverging length scale associated with the glass transition, similar perhaps to the correlation length in a magnetic transition, would enhance our understanding of the glass transition and of the glassy state.

Perhaps the most convincing argument favoring the view that there is an underlying phase transition is due to Kauzmann.[1] The liquid has a larger specific heat and therefore a higher rate of entropy increase with temperature than does the crystal. If one extrapolates to low temperature, the liquid entropy passes below that of the crystal at a nonzero temperature. This seems physically implausible, although it does not violate any thermodynamic laws. However, further extrapolation of the entropy curve to zero temperature results in a negative entropy. We cannot ignore such a situation. One plausible resolution to the paradox is to hypothesize the existence of a phase transition at or above the temperature at which the liquid and solid entropies cross. Indeed, in all known cases the apparent glass transition intervenes before this situation arises.

Experiments to date have been unsuccessful in identifying the glass transition as a thermodynamic transition with a corresponding divergent length scale. Susceptibility measurements, including very detailed studies of dielectric response[2] for a number of glass formers over a broad range of temperature and frequency, indicate no singularites near the transition temperature; one might expect to see such singularities in a system whose correlation length is diverging. Studies of nonlinear susceptibilities,[3] such as have been successful in identifying a correlation length in spin glasses,[4] have likewise shown no evidence of a diverging length scale at the structural glass transition. In another attempt to find a correlation length characterizing the transition, a recent experiment[5] employed polystyrene spheres of various sizes to probe the viscosity of an organic glass former at different length scales. This study also yielded a null result and thus contradicted an earlier measurement[6] which had reported a difference between the microscopic and macroscopic viscosities.

Computer simulations are well suited to the task of searching for different order parameters in condensed matter systems. Molecular dynamics techniques provide, in principle, complete information about the system under study, including the position, velocity, and potential energy of each particle. With such data, one can calculate correlation functions and thermodynamic parameters with relative ease. Moreover, computer simulations make accessible some physical parameters, such as the frequency-dependent thermal conductivity $\kappa(\omega)$ and the constant volume specific heat c_v, which are ordinarily quite difficult to measure in the laboratory.

While simulation studies offer us a powerful tool, a number of caveats must be noted. Statistical mechanics concerns itself largely with large numbers of particles, while present day computers allow meaningful simulations of far fewer than the 10^{23} particles we would ideally want. (The simulation presented here contains 500 particles.) Also, even the longest computer runs, which may take days or weeks of clock time, are limited to the equivalent of nanoseconds from the point of view of the system being simulated. Despite these drawbacks, simulation "experiments" of the glass transition[7-14] have produced data in good agreement with conventional measurements in several key respects. Fox and Andersen[7] have demonstrated that the density of the simulated glass state is a function of the cooling rate, and that this density shows hysteresis as the system is heated and cooled. They also found a departure at the glass transition temperature from the liquid state behavior of both volume and enthalpy versus temperature. Grest and Nagel[8] have seen a frequency-dependent specific heat in their simulation. Mountain and Thirumalai[9] see evidence of nonexperimental relaxation, with a relaxation rate which diverges at finite temperature. All of these signatures have been seen in actual glass formers.

This paper is divided into six sections: in the next section, we discuss the simulation itself, summarizing the molecular dynamics technique. We then present new data on the frequency-dependent thermal conductivity and constant volume specific heat. A section on translational order follows, in which we examine the correlation of the particle positions over time and space. In Sec. V we investigate the possibility of orientational ordering, that is the correlations between nearest-neighbor bond angles. A discussion section concludes the paper.

II. THE SIMULATION

The simulation we present in this paper is the same as that used by Grest and Nagel.[8] This consists of both constant pressure and constant volume molecular-dynamics simulations of 500 argonlike particles in a box with periodic boundary conditions. The particles interact via a modified Lennard-Jones potential

$$U_{ij}(r)=4\varepsilon S(r)\left[\left[\frac{\sigma_{ij}}{r}\right]^{12}-\left[\frac{\sigma_{ij}}{r}\right]^{6}\right]. \tag{1}$$

$U_{ij}(r)$ is the interaction energy between particles i and j, which are separated by a distance r, ε is the energy scale of the interaction, and σ_{ij} is the sum of the radii of particles i and j. $S(r)$ is a smoothing function which brings the interaction energy smoothly to zero at finite separation:

$$S(r)=\begin{cases}1, r<r_l\\ 1-(r-r_l)^2(3r_c-r_l-2r)/(r_c-r_l)^3, r_l<r<r_c\\ 0, r>r_c\ ,\end{cases} \tag{2}$$

where we have used $r_l=1.9\sigma_{ij}$ and $r_c=2.3\sigma_{ij}$. Forcing the potential to zero at finite r greatly reduces the number of particle-particle interactions that need to be calculated, allowing for a system of more particles and longer runs. However, truncating the potential, as is often done, produces discontinuities in either $U_{ij}(r)$ or its derivative, and decreases the degree to which energy is conserved. The form for $S(r)$ shown in Eq. (2) allows us to run the simulation for very long times (on the order of 800,000 time steps), while at the same time conserving energy to one part in 10^6. In order to inhibit crystallization, the system is a binary alloy, with 80% large particles of diameter σ, and 20% small particles of diameter 0.8σ. σ_{ij} in the potential thus has the values: $\sigma_{ij}=\sigma$ between two large particles, $\sigma_{ij}=0.9\sigma$ between a large and a small particle, and $\sigma_{ij}=0.8\sigma$ between two small particles. Both large and small particles have the same mass, m.

All quantities quoted in this paper are stated in terms of the natural units of the potential; thus distances are measured in units of σ, temperatures are given as $T^*=Tk_B/\varepsilon$ (k_B is Boltzmann's constant), and time is given in units of $\tau=\sigma(m/\varepsilon)^{1/2}$. In our simulation we used a time step $\Delta t=0.0025\tau$. We studied the system at several different temperatures, ranging from $T^*=1.00$ to $T^*=0.02$. The apparent glass transition temperature is about $T_g^*\approx 0.40$, while the freezing temperature is $T^*=0.80$ at $\rho^*=0.95$ (ρ^* is the density in units of σ^{-3}). Thus, $T^*=1.00$ is a well equilibrated liquid, and $T^*=0.17$ is a solid, virtually devoid of structural rearrangement on the time scale of this simulation.

Cooling of the system (which is done at constant pressure) is accomplished by lowering the temperature of a heat bath, to which the system is weakly coupled, by $\Delta T^*=0.1$ and equilibrating for 60τ. The process is repeated until the desired temperature is reached, at which point the coupling to the heat bath is turned off. The end product of this cooling process is used as the starting state for each of the long microcanonical constant volume and constant pressure runs. In the constant pressure simulation, the walls are allowed to move, and the wall mass is taken to be the same as that of the particles so that the wall motion occurs at high frequency and does not affect the low-frequency dynamics in which we are principally interested.

The simulation shows many indications of a glass transition and of glassy dynamics. The system can be quenched into a low-temperature solid which remains amorphous over the entire duration of the simulation run. As the glass transition temperature $T_g^*\approx 0.40$ is approached, the diffusion constant goes smoothly to zero, and the specific heat drops precipitously over a narrow temperature interval. Enthalpy, which decreases linearly, and density, which increases linearly, with decreasing temperature in the liquid, both begin to deviate smoothly from the liquid behavior at T_g^*. The specific heat (at both constant pressure and constant volume) has also been observed to be frequency dependent. A frequency-dependent c_p is in agreement with experiments[15,16] which show that low-frequency relaxation modes contribute significantly to the enthalphy. These results were discussed in greater detail by Grest and Nagel.[8]

III. THERMODYNAMICS AND TRANSPORT

A. Thermal conductivity

Several theories which have been developed to include the presence of slowly relaxing modes in a glass conclude that the thermal conductivity should become frequency dependent in the vicinity of the glass transition. Jäckle[17] presents a phenomenological model based on thermoviscoelastic theory which assumes that configurational modes, in addition to phonons, conduct heat. The result is a thermal conductivity with a small (a few percent) frequency-dependent component. Oxtoby[18] describes a hydrodynamic theory which also includes slowly relaxing internal modes. He concludes that the thermal conductivity is frequency- and wave-vector dependent. In his model, an apparent frequency-dependent specific heat is regarded merely as a convenient way to allow the inclusion of the time development of the slow modes.

Generally, laboratory experiments measure some combination of c_p and κ. Only recently[16] has it been possible to distinguish clearly between the two quantities. While these results have shown a very distinct dependence of the specific heat on frequency, no frequency dependence was found in the thermal conductivity to within the experimental error of a few percent. The simulations of Grest and Nagel[8] have already shown a frequency-dependent specific heat (both c_p and c_v). The existence of a frequency dependence in the measured value of c_v appears to refute the contention of Zwanzig [19] that the only frequency dependence should occur in $(c_p - c_v)$. We present here a calculation of the time dependence of the thermal conductivity.

We have calculated the thermal current correlation function[20] (derived from the Kubo-Greenwood formula[21]):

$$C_E(t) = \frac{1}{3Vk_BT}\langle J_{Ex}(0)J_{Ex}(t) + J_{Ey}(0)J_{Ey}(t) + J_{Ez}(0)J_{Ez}(t)\rangle \ , \tag{3}$$

where the thermal current J_{Ex} is defined by

$$J_{Ex} = \left[\sum_{i=1}^{N}\frac{mv_i^2}{2} + \sum_{i=1}^{N}\sum_{j\neq i}\frac{1}{2}U(r_{ij})\right]v_{xi} - \sum_{i=1}^{N}\sum_{j\neq i}\frac{\partial U(r_{ij})}{\partial x_{ij}}\frac{1}{2}(\mathbf{r}_{ij}\cdot\mathbf{v}_i) \ . \tag{4}$$

V is the volume of the system, v_i is the velocity of particle i, v_{xi} is the x component of that velocity, r_{ij} is the separation between the particles, and the derivative is taken with respect to the x component of the particle separation. J_{Ey} and J_{Ez} are similarly defined. The frequency-dependent thermal conductivity is

$$\kappa(\omega) = \int_0^\infty C_E(t)e^{i\omega t}dt \ . \tag{5}$$

The correlation functions, $C_E(t)/C_E(0)$, for the constant volume simulation are plotted in Fig. 1(a) for a variety of temperatures. We observe the same qualitative results as Amar and Mountain[20] found for the soft-sphere model. Note that at each temperature, the correlation function decays to zero within a very short time. The relaxation time for these decays is approximately 0.5τ, independent of temperature. This is just below a characteristic period for a phonon in the system. This result is obtained in the same range of temperatures for which the specific heat was found to be frequency dependent.

As in Ref. 8, in order to find the frequency-dependent specific heat we first calculate the kinetic energy correlation function $K(t)$:

$$K(t) = \frac{N\langle[T(t+s)-T][T(s)-T]\rangle_s}{T^2} \ , \tag{6}$$

where $T(s)$ is the instantaneous temperature at time s. T is the average temperature, and the angled brackets represent an average over starting times s. The specific heat in the microcanonical ensemble is related to $K(t)$ by

$$c(\omega) = \left[\frac{2}{3} - \int_0^\infty K(t)e^{i\omega t}dt\right]^{-1} \ . \tag{7}$$

We show in Fig. 1(b) the curves of $K(t)/K(0)$ for the same temperatures as in Fig. 1(a). Notice that $C_E(t)/C_E(0)$ decays to zero, whereas in the vicinity of the glass transition ($T^* = 0.40$ and 0.32), $K(t)/K(0)$ does not. This indicates that there is considerable time (or frequency) dependence in the specific heat, but not in the thermal conductivity below a typical phonon frequency. There is very little statistical uncertainty in the result, as

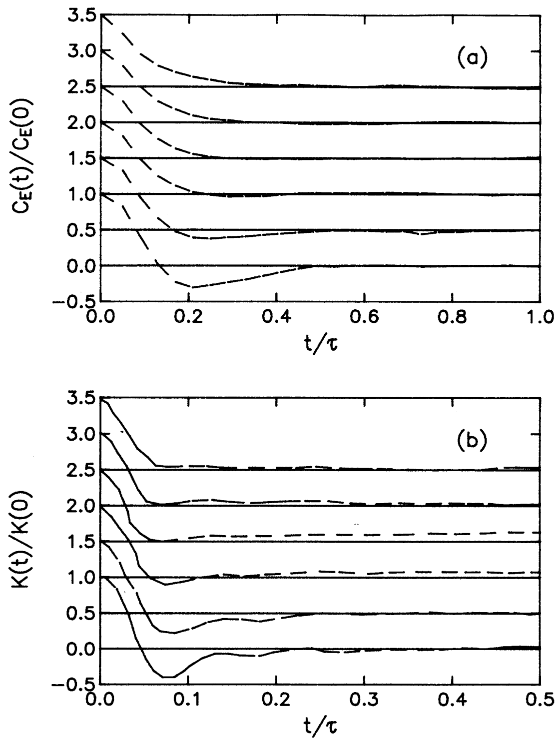

FIG. 1. (a) $C_E(t)/C_E(0)$, the thermal current correlation function calculated at constant volume vs time for different temperatures. (b) The kinetic energy correlation function $K(t)/K(0)$ calculated at constant volume vs time for different temperatures. In both (a) and (b), the dashed curves represent, from top to bottom, $T^* = 0.81$, 0.52, 0.40, 0.32, 0.17, and 0.02. For clarity, the curves are offset vertically from one another by 0.5.

the correlation functions are well averaged and show no features (to better than 1%) in the $t > 0.5\tau$ range. The simulation thus extends the range of validity of the laboratory result, and does so with considerably less uncertainty.

B. Constant pressure and constant volume specific heats

Comparing the constant pressure and constant volume specific heats c_p and c_v, with the coefficient of thermal expansion α, and the isentropic compressibility κ_s allows us to gauge the degree to which the two simulations (constant pressure and constant volume) represent the same system. Since the constant pressure simulation includes movable walls which interact with the particles, it is possible that the dynamics of the system may be adversely affected. In equilibrium,

$$(c_p - c_v)\frac{c_p}{c_v} = \frac{T\alpha^2}{\rho\kappa_s} , \tag{8}$$

where α and κ_s can be calculated from[22–24]

$$\kappa_s = \frac{1}{\bar{V}T}\langle [V(s) - \bar{V}][V(s) - \bar{V}] \rangle_s \tag{9}$$

and

$$\alpha = -c_p \frac{N}{\bar{V}T^2}\langle [T(s) - T][V(s) - \bar{V}] \rangle_s . \tag{10}$$

ρ is the density, $V(s)$ is the volume at time s, and $\bar{V}$ is the time-averaged volume. The expressions in angled brackets are averaged over the time s. α and κ_s are plotted as functions of T^* in Fig. 2. As can be seen in Fig. 3, the equality of Eq. (8) is very closely obeyed. This indicates that the constant volume and constant pressure simulations can be treated as the same system under different external conditions. These results are consistent with the assumption that the dynamics of the walls of the box do not compromise the simulation.

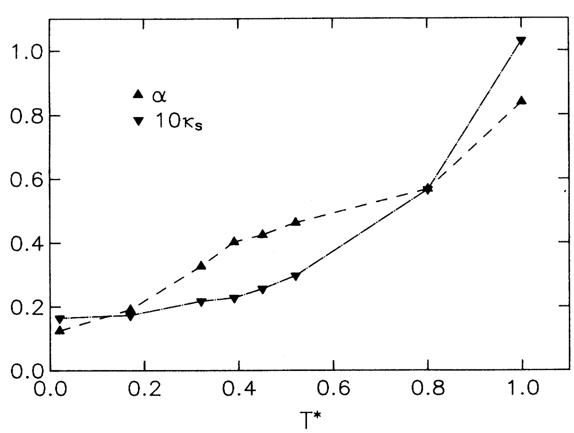

FIG. 2. Coefficient of thermal expansion, α, and isentropic compressibility, κ_s, vs temperature. The compressibility has been multiplied by 10 for clarity. The solid and dashed lines are guides to the eye.

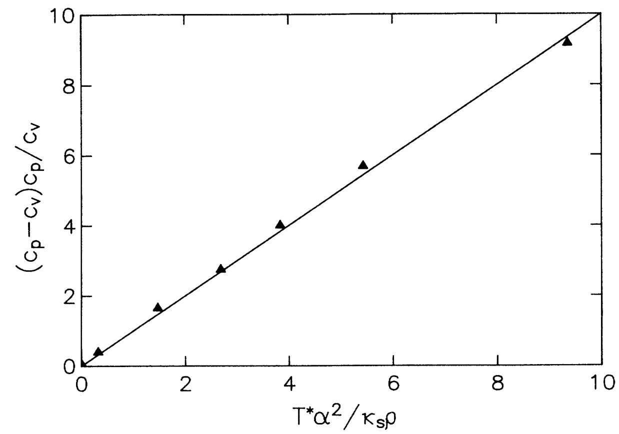

FIG. 3. $(c_p - c_v)c_p/c_v$ vs $T^*\alpha^2/\kappa_s\rho$. The comparison shows the equivalence between the simulations of constant pressure and constant volume.

IV. TRANSLATIONAL ORDERING

While glasses lack the long-range translational order of crystals, the possibility of persistent short- or medium-range order still exists. We look, therefore, for evidence of freezing into long-lived clusters of solid material within the liquid, which grow as the system is cooled through the transition.

The space-time correlation function, or density-density correlation function[25]

$$G(r,t) = \frac{1}{N}\left\langle \sum_{i=1}^{N}\sum_{j=1}^{N} \delta(|\mathbf{r}_i(t+s) - \mathbf{r}_j(s)| - r) \right\rangle_s \tag{11}$$

measures the average probability of finding a particle at time t, a distance r away from where a particle was at time 0. The angled brackets indicate an average over starting times, s. The δ function is discretized, so that $\delta(r)=1$ for $0 < r \le \Delta r$, and $\delta(r)=0$ otherwise. We note that, beyond the obvious smoothing at large values of Δr, none of the results in this paper are affected by the choice of bin width Δr.

The pair distribution function[25]

$$g(r) = \frac{1}{\rho_0} G(r, t=0) \tag{12}$$

indicates the direction-averaged local density a distance r from the average particle (ρ_0 is the average density). When analyzing results for $G(r,t)$, we focus on values of r which correspond to peaks in $g(r)$, that is, nearest neighbors, next nearest neighbors, and so on, since these are the positions where most particles reside and where the best averaging can be accomplished.

Figure 4 shows $g(r)$ for six temperatures studied. The most notable feature is the broad peaks, characteristic of amorphous systems. A split second peak has often been

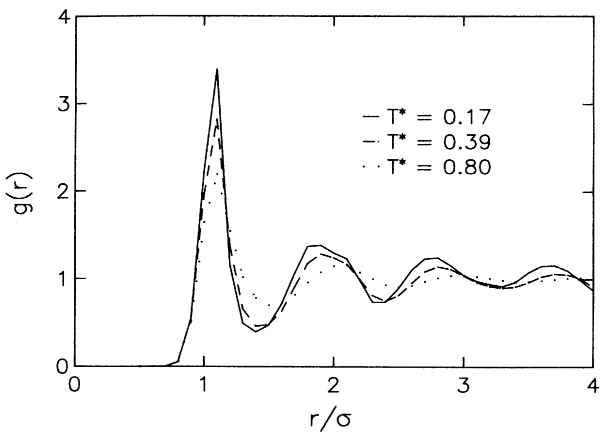

FIG. 4. The pair correlation function, $g(r)$, vs distance for the temperatures $T^*=0.17$, 0.39, and 0.80. $g(r)$ is normalized to unity at large values of r.

pointed out as a hallmark of glassiness,[12] and we see some evidence of such a peak, albeit a diffuse one, particularly at the lowest temperature, $T^*=0.17$. The split second peak is not as sharp as those seen by others because our system is a binary alloy. In a monatomic system we found a more sharply split second peak. Notice also the growth of the peaks, in particular the first peak, as the temperature decreases.

Figure 5 shows $G(r,t)/G(r,0)$ for the peak values of r. We include the first four peaks in $g(r)$, since they are well defined and are contained wholly within the box which defines the system size. At all temperatures and peak positions, there is an initial very fast relaxation, followed by a slower decay to a nonzero asymptote. We have identified the short-time behavior as motion due to vibrations about local equilibrium positions. The structural relaxation shown by the slower decay is what interests us. At high temperature the relaxations all follow a smooth curve. The relaxation at the lowest temperature, $T^*=0.17$, does not follow any smooth form as was found at higher temperatures. This is likely because at this low temperature particles relax extremely slowly so that the entire simulation spans less than one decay time. Sufficient averaging of the data is thus not possible at $T^*=0.17$. If we look at $G(r,t)/G(r,0)$ for values of r corresponding to the minima of $g(r)$, the correlation functions grow with increasing t, but still show much the same exponential approach to their final values as do the peaks. Since these off-peak correlation functions convey the same information as the peaks, we focus only on the peaks. We again note that the choice of a binning width Δr does not affect the structure of $G(r,t)$.

We have fit the correlation functions to a simple exponential with a nonzero asymptote:

$$G(r,t)=A[G_\infty-(G_\infty-1)\exp(-t/\tau_G)] . \qquad (13)$$

G_∞ is the infinite-time asymptote, and (AG_∞) defines the amount by which the correlation function decays from $t=0$ to $t=\infty$. τ_G is the exponential relaxation time of $G(r,t)$. Since the first few time points for each correlation function are primarily due to vibrational relaxation, we exclude these points from our fits. We typically ig-

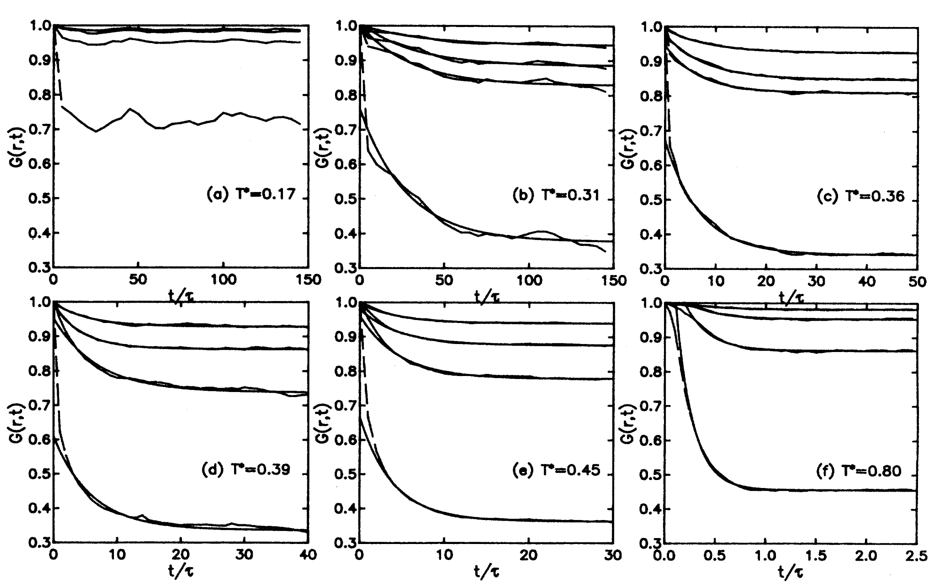

FIG. 5. The space-time correlation function, $G(r,t)$ vs time. Figures 5(a)–5(f) represent $T^*=0.17$, 0.31, 0.36, 0.39, 0.45, and 0.80, respectively. At each temperature, the curves, from bottom to top, correspond to the first through fourth peaks. The smooth curves are the best fits to the exponential form of Eq. (13). The data for $T^*=0.17$ (a) could not be fit to the functional form.

nore the data for $t < \tau$; we have checked that the particular choice of a low-time cutoff does not change the fitted value of τ_G (the fit parameter which interests us most) by more than a few percent. The structural relaxation portions of all of the correlation functions are observed to be exponential, and are fit by Eq. (13) quite well.

We have looked for an increase in the relaxation time measured at different values of r at different temperatures. The existence of such an r-dependent relaxation time would indicate the presence of an underlying length scale. If the system were freezing into progressively larger clusters as we cool through the transition, we would see all four peaks with short relaxation times at high temperatures; as the temperature is lowered, the curves for small values of r would begin to increase before those corresponding to larger values of r. Figure 6 shows τ_G, the fitted exponential decay constant for the first four peaks in $g(r)$, plotted as a function of temperature. Notice that all four peaks have roughly the same relaxation rates at each temperature, with very fast relaxation at high temperature and relaxation too slow to quantify at the lowest temperature. We see here no length scale associated with the glass transition. Instead, we must conclude that by this probe, at least, the system simply becomes more and more viscous, regardless of the length scale at which we view it.

While $G(r,t)$ cannot be measured directly, its spatial Fourier transform $F(q,t)$ can be determined by neutron spin-echo scattering. Mezei, Knaak, and Farago[26] have measured $F(q,t)$ for the ionic system $Ca_{0.4}K_{0.6}(NO_3)_{1.4}$ for times less than 2×10^{-9} sec. By using inelastic neutron scattering, one can also determine the temporal Fourier transform, $S(q,\omega)$. All of these measurements indicate that, as expected, the relaxation time is increasing as T decreases. In accord with our results for $G(r,t)$, they give no indication of a correlation length which increases as the temperature is reduced. Similar results have also been obtained from molecular dynamics simulations of binary Lennard-Jones systems by Ullo and Yip. The curves for $F(q,t)$ obtained in our simulation are very similar to those of Ullo and Yip.[27]

V. ORIENTATIONAL ORDERING

Following the work of Steinhardt, Nelson, and Ronchetti[28] and Jónnson and Andersen,[29] we turn our attention to bond orientational ordering. Motivated by ideas such as hexatic ordering in two-dimensional solids, they looked not for the sort of translational ordering of particles apparent from the density-density correlation function, but for correlations in the nearest-neighbor bond angles. The procedure involves evaluating the spherical harmonics, $Y_{lm}(\theta,\varphi)$, using the bond angles as arguments.

By averaging over bonds, they quantified the degree to which the bonds, on average, display the general symmetry of the different spherical harmonics used. Random bond angles tend to cancel out in the average over bonds of the spherical harmonics, while correlated bond angles, no matter where they are located in the system, add coherently.

In our simulations we first evaluate

$$Q_l = \left[\frac{4\pi}{2l+1} \sum_{m=-l}^{l} \left| \frac{1}{N_{\text{bonds}}} \sum_{i=1}^{N_{\text{bonds}}} Y_{lm}(\theta_i,\varphi_i) \right|^2 \right]^{1/2} . \tag{14}$$

While Q_l does not by itself measure any length scale dependence in the orientational ordering, it indicates the sort of angular symmetry present in the sample. This quantity was calculated by Steinhardt *et al.*, and calculating Q_l here will serve as an additional basis for comparison between our results and theirs. The sum is taken over all bonds labeled by i. In Fig. 7 Q_l is evaluated for a range of l values and temperatures. For the purposes of this and all other bond correlation functions, nearest neighbors are taken to be those particles whose separation is less than the value of r corresponding to the first

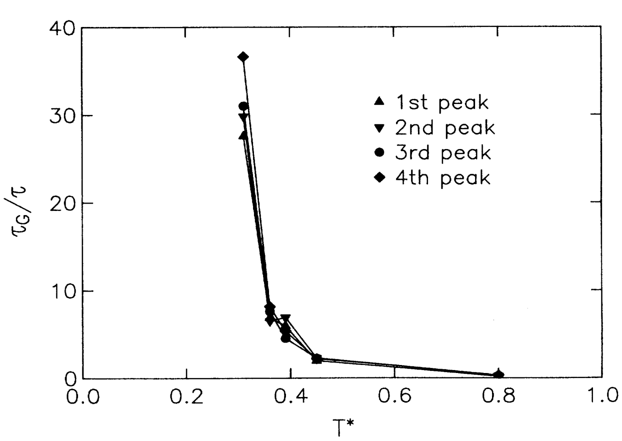

FIG. 6. The exponential relaxation time, τ_G, obtained from fits of the data in Fig. 5 to the form of Eq. (13). Notice that all peaks show approximately the same relaxation time at each temperature, and that the relaxation times increase at low temperatures.

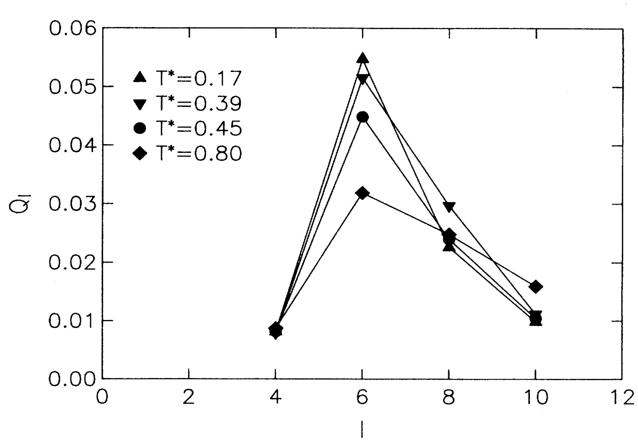

FIG. 7. The quantity Q_l for four temperatures. Notice the growth of $Q_{l=6}$, corresponding to threefold symmetry, as the temperature decreases.

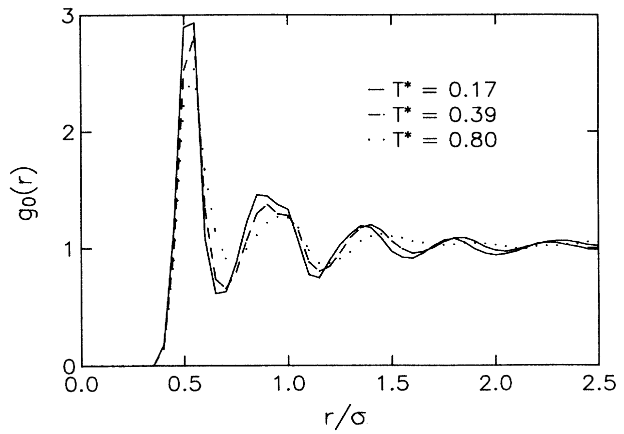

FIG. 8. The bond pair correlation function, $g_0(r)$, vs distance for the temperatures $T^*=0.17$, 0.39, and 0.80. $g_0(r)$ is normalized to unity at large values of r.

minimum in $g(r)$. The position of the bond is the midpoint of the line joining the two particles, and the polar and azimuthal angles θ and φ are taken with respect to a coordinate system fixed by the box. By averaging over all m values, we insure that the choice of a particular coordinate system does not affect the results.

The important feature to note in Fig. 7 is the steady growth in the $l=6$ peak as the system is cooled. This $l=6$ peak indicates threefold symmetry in the bond angles, and along with an $l=10$ peak, is characteristic of the icosahedron, a locally energetically favorable configuration for Lennard-Jones solids. While the data for Q_l does suggest icosahedral symmetry, it is not the most sensitive test of such local ordering. Since icosahedra (unlike cubes, for example) cannot tessellate space, we should not expect icosahedral ordering to be present over length scales much greater than the nearest-neighbor spacing. The average in Q_l, which is taken over the entire system, is therefore less than would be expected for a pure icosahedron. Our results agree qualitatively with those of Steinhardt *et al.*

We now expand the search for bond orientational ordering by looking at correlations between bonds in both time and space. We first examine the spatial correlation of bond positions. In direct analogy with the particle space-time correlation function, we look at

$$G_0(r,t)=\left\langle \sum_{i=1}^{N_{\text{bonds}}(t+s)} \sum_{j=1}^{N_{\text{bonds}}(s)} \delta(|\mathbf{R}_i(t+s)-\mathbf{R}_j(s)|-r)\right\rangle_s \tag{15}$$

where $\mathbf{R}_i$ and $\mathbf{R}_j$ denote bond positions, and the angled brackets again denote an average over starting times s.

We undertake exactly the same sort of analysis with $G_0(r,t)$ as we did with $G(r,t)$. $g_0(r)$ is analogous to $g(r)$ and is simply the probability of finding a bond a distance r away from any other bond. Figure 8 shows

$$g_0(r)=G_0(r,t=0)/r^2$$

for three temperatures studied. We see exactly the same

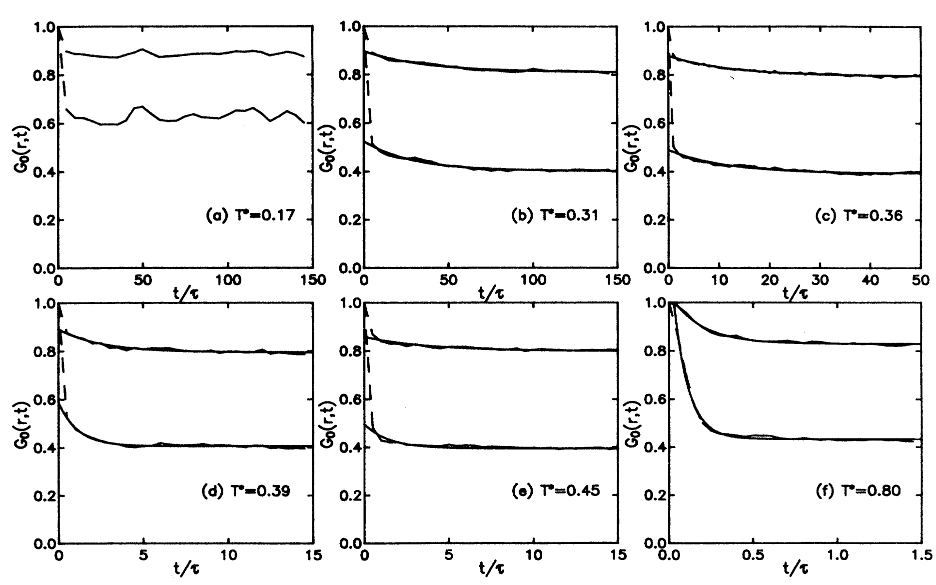

FIG. 9. The bond correlation function $G_0(r,t)$ vs time. Figures 9(a)–9(f) represent $T^*=0.17$, 0.31, 0.36, 0.39, 0.45, and 0.80, respectively. At each temperature, the top curve corresponds to the second peak, and the bottom curve corresponds to the first peak. The smooth curves are the best fits to Eq. (13). The data for $T^*=0.17$ (a) could not be fit to the functional form.

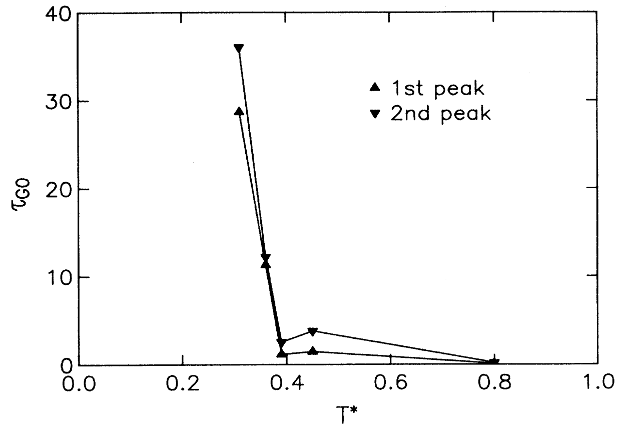

FIG. 10. The exponential relaxation time, τ_{G0}, obtained from fits of the data in Fig. 9 to the form of Eq. (13). Notice that both peaks show approximately the same relaxation time at each temperature, and that the relaxation time increases as the system is cooled.

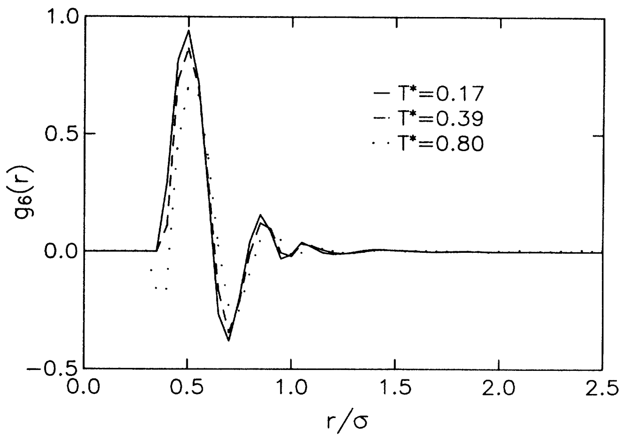

FIG. 11. The function $g_6(r)$ vs distance for the temperatures $T^*=0.17$, 0.39, and 0.80. The general oscillatory shape of the curves is in marked contrast to the data in Ref. 28. Higher temperatures have higher peaks and deeper troughs than do the lower temperatures.

qualitative behavior as in $g(r)$: broad peaks which grow with decreasing temperature and a split or broadened second peak. Notice that the positions of all of the peaks in $g_0(r)$ occur at roughly half the distance from the origin as do the corresponding peaks in $g(r)$. This is reasonable since, if we consider the distances between nearest-neighbor bonds in an hcp lattice, for example, the bond positions also form an hcp lattice with half the original lattice spacing.

In Fig. 9, we see for $G_0(r,t)$ qualitatively the same behavior as in $G(r,t)$. In this case, however, only the first two peaks in $g_0(r)$ yield a definable decay in $G_0(r,t)$ as a function of t. Peaks beyond the first two, while well defined in $g_0(r)$, do not yield well-characterized relaxation curves in $G_0(r,t)$. As with $G(r,t)$, before the structural relaxation begins to be observable we see an initial very fast relaxation which we attribute to vibrational motion. We fit the correlation functions [ignoring the first few time points, as with the fits to $G(r,t)$] to the exponential form of Eq. (13), where the decay time is now denoted as τ_{G0}. τ_{G0} is plotted as a function of temperature in Fig. 10. As for $G(r,t)$, there is no indication in $G_0(r,t)$ of a length scale since both peaks for a given temperature relax at roughly the same rate.

We now examine the spatial and temporal correlations between bond angles. The correlation function we use is

$$G_6(r,t)=\frac{\left\langle \frac{4\pi}{13}\sum_{m=-6}^{6}\sum_{i=1}^{N_{\text{bonds}}(t+s)}\sum_{j=1}^{N_{\text{bonds}}(s)} Y_{6m}(\theta_i,\varphi_i)Y^*_{6m}(\theta_j,\varphi_j)\delta(|\mathbf{R}_i(t+s)-\mathbf{R}_j(s)|-r)\right\rangle_s}{G_0(r,t)}\,, \tag{16}$$

which is a generalization of the function $G_6(r)$ used by Stienhardt *et al.*[28] We sum over all bonds i at time $t+s$ and bonds j at time s. The denominator $G_0(r,t)$ normalizes out the varying contribution to the sum at different values of r due to different bond densities.

Figure 11 shows $g_6(r)\equiv G_6(r,t=0)$. [What we call $g_6(r)$ is exactly the function $G_6(r)$ as specified by Steinhardt *et al.*[28] Our algorithm for computing $g_6(r)$ differs from theirs as will be discussed below.] Notice that $g_6(r)$ is a damped oscillatory function, with sizable excursions to negative values. This result is in marked contrast to the results of Steinhardt *et al.*, who see a smooth monotonic decay of $G_6(r)$ at all temperatures.

In addition to a disagreement with Steinhardt *et al.* as to the shape of the curves at each temperature, we also find a different temperature dependence in $G_6(r)$. They fit the $G_6(r)$ data to an exponential

$$[G_6(r)\sim\exp(-r/\xi_6)]\,,$$

and treat ξ_6 as a correlation length. As the system is cooled, they see a growth in ξ_6 which diverges at the glass transition temperature. In contrast, we cannot fit $G_6(r)$ with a simple function of the form they used since our data are dominated by oscillatory behavior. We therefore have to treat each peak position separately. We see very little difference in $g_6(r)$ from one temperature to another. The peaks in $g_6(r)$ remain in roughly the same positions, with only small shifts to lower values of r as the temperature drops. At $T^*=0.80$, we also see a trough in $g_6(r)$ preceding the first peak, which is not present at other temperatures.

Since our results differ so markedly with those of Steinhardt *et al.*, we have attempted to reproduce their results using the coarse-graining prescription contained in their paper. Their procedure involves subdividing the system into a lattice of $16 \times 16 \times 16$ boxes. Each bond makes a contribution to the sum of the spherical harmonics at the eight vertices of the box in which it is contained. The contribution of the bond to a given vertex is weighted by its proximity to the vertex. It is the $(16 \times 16 \times 16)$ vertices which are then correlated to give the coarse-grained function $G_6(r)$.

The results for the coarse-grained $G_6(r)$ are shown in Fig. 12 by the curves denoted "vertex coarse grained." Notice that much of the structure in $G_6(r)$ is washed out by the coarse graining, and that this method yields results closer to the smooth monotonic decay seen by Steinhardt *et al.* They also mention a Fourier-transform technique, which may have further filtered out the oscillations in $G_6(r)$. Even using the coarse-graining procedure, we still do not see any dramatic temperature dependence, and we still cannot fit our data with a smooth monotonically decreasing function. Figure 12 also contains curves calculated using an alternate coarse-graining algorithm. In this second case, each bond contributes an unweighted amount to the center of the box in which it is contained. The $(16 \times 16 \times 16)$ centers are then correlated. These curves, labeled "center coarse grained" are almost identical to the results obtained by our previous coarse-graining procedure.

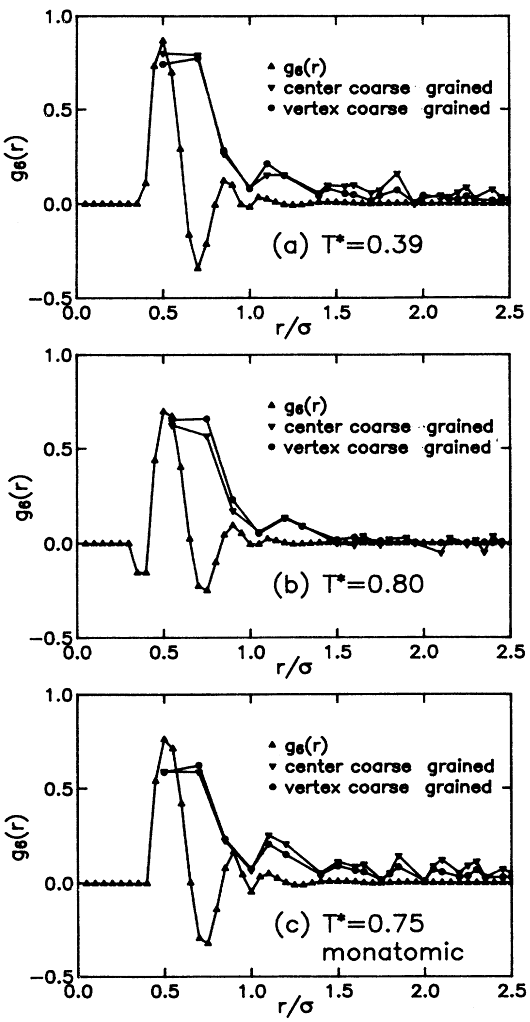

FIG. 12. $g_6(r)$ compared with the corresponding coarse-grained quantity specified in Ref. 28. Figures 12(a) and 12(b) represent $T^* = 0.39$ and 0.80, respectively, and 12(c) represents a monatomic system at $T^* = 0.75$. The center and vertex coarse-graining procedures are discussed in the text. Some of the structure in $g_6(r)$ is evidently averaged out by coarse graining.

In order to make a more direct comparison with the results of Steinhardt *et al.*, we have also calculated $g_6(r)$ for a monatomic system at $T^* = 0.75$, which is below its glass transition temperature. These results are shown in Fig. 12(c). Our results for this system are much the same as for the binary system and show strong oscillations as a function of r. They thus differ considerably from the course-grained results of Steinhardt *et al.* We also show in that figure the two course-grained averages which again tend to wash out the oscillations. It is not clear to us that the course graining, which removes most of the structure in the curves, is justified. We will not use any coarse graining in the subsequent calculations.

Figure 13 shows $G_6(r,t)$ for six temperatures studied. We plot correlation functions for only the first two peaks in $g_6(r)$. There are three discernable peaks in $g_6(r)$, but the third peak yields no well-defined relaxation in $G_6(r,t)$. At all temperatures, both peaks show essentially the same form of exponential decay as was seen in the other correlation functions. The first peak here shows a much longer decay time than is shown by the second peak.

The $G_6(r,t)$ data were fitted to the same exponential form [Eq. (13)] as were the other correlation functions. As the temperature decreases, the decay times, τ_{G6}, for both peaks increase, but we see no indication of preferential freezing at any length scale at any temperature. The ratio of τ_{G6} for the first peak to that of the second peak shows no meaningful trend, and is not monotonic in temperature. Results for the decay times τ_{G6} are summarized in Fig. 14. Note that the second peak shows no relaxation at temperatures $T^* \leq 0.31$, and at $T^* = 0.17$ even the first peak does not decay. We conclude that the data do not support the notion of length scale-dependent freezing in of bond-orientational order.

VI. CONCLUSIONS

The molecular dynamics data indicate that the thermal conductivity of the glass is independent of frequency, while the specific heat is clearly frequency dependent. Our simulation is thus in agreement with the only laboratory measurements to have determined the two quantities separately. Apparently, the current models for heat transport in glasses have overemphasized the importance of the frequency dependence of the thermal conductivity.

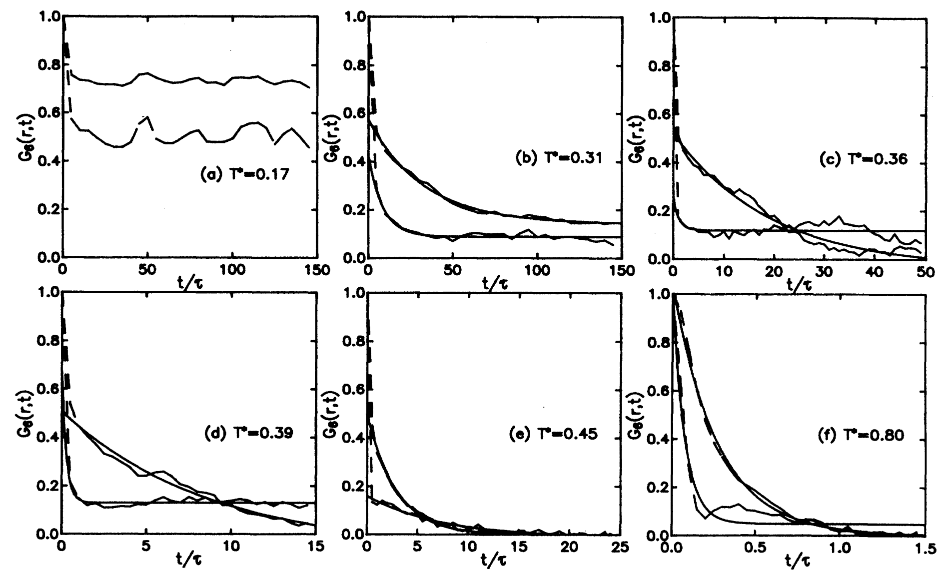

FIG. 13. The bond correlation function $G_6(r,t)$ vs time. Figures 13(a)–13(f) represent $T^*=0.17$, 0.31, 0.36, 0.39, 0.45, and 0.80, respectively. At each temperature, the top curve corresponds to the second peak, and the bottom curve corresponds to the first peak. The smooth curves are the best fits to Eq. (13). The data for $T^*=0.17$ could not be fit meaningfully to that functional form.

Comparison of the constant pressure and constant volume simulations indicates that the two represent the same system, and that the computational mechanism needed for the constant pressure simulation does not adversely affect the results. This encouraging result shows that simulations can be used to study both constant pressure systems, which are experimentally accessible, as well as constant volume systems, which ordinarily are not.

We have examined the molecular dynamics data for evidence of a correlation length by studying both translational and bond-orientational ordering. We find no evidence of length scale-dependent freezing as the simulated system is cooled through the glass transition. The limitations inherent in computer simulations have already been noted, but we do not believe that the lack of a positive result is a direct result of these limitations. While the system is quite limited in size (the box contains about eight particles on a side), this is the scale at which we would have expected to see correlated clusters of particles or bonds. The correlation functions we studied were allowed to decay to their asymptotic values, so the relatively short-time duration of the simulation should likewise not have obscured the results. Had we simulated a larger system for a longer time, we presumably would have seen much the same behavior but with less noise.

The conclusion we draw from this work is that if there is a correlation length in glassy systems, it does not show itself in the density-density correlation function, nor in the orientational correlation functions we have calculated. These results parallel the laboratory experiments, which also have been unable to identify a diverging length scale.

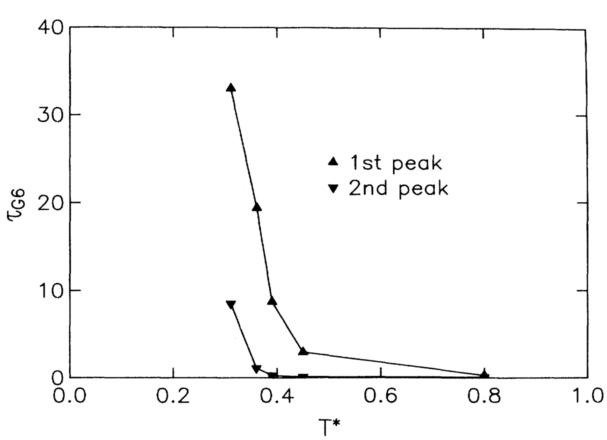

FIG. 14. The relaxation time, τ_{G6}, obtained from exponential fits of the data in Fig. 13. Notice that the first peak has a larger relaxation time than the second peak at each temperature, and that the relaxation times increase as the system is cooled.

ACKNOWLEDGMENTS

We thank P. K. Dixon and L. Wu for helpful discussions. This work was supported in part by the National Science Foundation under Grant No. DMR 88-02284, and by the National Center for Supercomputing Applications at The University of Illinois at Urbana-Champaign.

[1]W. Kauzmann, Chem. Rev. **43**, 219 (1948).

[2]P. K. Dixon, L. Wu, S. R. Nagel, B. D. Williams, and J. P. Carini, Phys. Rev. Lett. **65**, 1108 (1990); L. Wu, P. K. Dixon, N. Menon, K. O'Brien, S. R. Nagel, B. D. Williams, and J. P. Carini (unpublished).

[3]Y. H. Jeong and S. R. Nagel (unpublished); L. Wu (unpublished).

[4]K. Binder and A. P. Young, Rev. Mod. Phys. **58**, 801 (1986).

[5]P. K. Dixon, S. R. Nagel, and D. Weitz (unpublished).

[6]Y. F. Kiyachenko and Y. I. Litvinov, Pis'ma Zh. Eksp. Teor. Fiz. **42**, 327 (1985) [JETP Lett. **42**, 266 (1985)].

[7]J. Fox and H. C. Andersen, J. Phys. Chem. **88**, 4019 (1984); Ann. N.Y. Acad. Sci. **371**, 123 (1981).

[8]G. S. Grest and S. R. Nagel, J. Phys. Chem. **91**, 4916 (1987).

[9]R. Mountain and D. Thirumalai (unpublished); Phys. Rev. A **36**, 3300 (1987); J. Phys. Chem. **93**, 6975 (1989).

[10]S. Nosé and F. Yonezawa, J. Chem. Phys. **84**, 1803 (1986).

[11]A. Rahman, M. J. Mandell, and J. P. McTague, J. Chem. Phys. **64**, 1564 (1976).

[12]H. R. Wendt and F. F. Abraham, Phys. Rev. Lett. **41**, 1244 (1978).

[13]B. Bernu, J. P. Hansen, Y. Hiwatari, and G. Pastore, Phys. Rev. A **36**, 4891 (1987).

[14]S. T. Chui, G. O. Williams, and H. C. Frisch, Phys. Rev. B **26**, 171 (1982).

[15]N. O. Birge and S. R. Nagel, Phys. Rev. Lett. **54**, 2674 (1985); N. O. Birge, Phys. Rev. B **34**, 1631 (1986).

[16]P. K. Dixon and S. R. Nagel, Phys. Rev. Lett. **61**, 341 (1988).

[17]J. Jäckle (unpublished).

[18]D. Oxtoby, J. Chem. Phys. **85**, 1549 (1986).

[19]R. Zwanzig, Annu. Rev. Phys. Chem. **16**, 67 (1965); (unpublished).

[20]J. G. Amar and R. D. Mountain, J. Chem. Phys. **86**, 2236 (1987).

[21]M. S. Green, J. Chem. Phys. **20**, 1281 (1952); M. S. Greene, J. Chem. Phys. **22**, 398 (1954); R. Kubo and K. Tomita, J. Phys. Soc. Jpn. **9**, 888 (1954).

[22]J. L. Lebowitz, J. K. Percus, and L. Verlet, Phys. Rev. **153**, 250 (1967).

[23]T. S. Y. Cheung, Mol. Phys. **33**, 519 (1977).

[24]J. Ray, H. W. Graben, and J. M. Haile, Nuovo Cimento **64B**, 141 (1981).

[25]N. E. Cusak, *The Physics of Structurally Disordered Matter: an Introduction* (IOP, Bristol, 1987).

[26]F. Mezei, W. Knaak, and B. Farago, Phys. Rev. Lett. **58**, 571 (1987).

[27]J. J. Ullo and S. Yip, Phys. Rev. Lett. **54**, 1509 (1985); Phys. Rev. A **39**, 5877 (1989); (unpublished).

[28]P. J. Steinhardt, D. R. Nelson, and M. Ronchetti, Phys. Rev. B **28**, 784 (1983); Phys. Rev. Lett. **47**, 1297 (1981).

[29]H. Jónsson and H. C. Andersen, Phys. Rev. Lett. **60**, 2295 (1988).